Influence of Iron Doping on Structural and Optical Properties of Nickel Oxide Nanoparticles

Nashiruddin Ahammed[1],*, **M. Mehedi Hassan[2]**

[1]*Department of Physics, Govt. General Degree College, Muragachha, Nadia, W.B. 741154, India*
[2]*Sensor and Actuator Division, CSIR-Central Glass and Ceramic Research Institute, Kolkata, W.B. 700032, India*

*Corresponding author: E-mail: nashiruddin73@gmail.com

Abstract

In this article, auto combustion prepared $Ni_{1-x}Fe_xO$ ($0 \leq x \leq 0.10$) nanoparticles (NPs) have been investigated for their structural, morphological and optical properties. X-ray diffraction (XRD) studies reveal that all Fe doped NiO samples crystallize in single phase without any impurity. The crystallite size monotonically decreases from 20 nm to 10 nm with increasing Fe substitution. Transmission Electron Microscope images represent that the synthesized NiO NPs with size around 28 nm. A red shift in UV-Vis spectra indicates that band gap can be tuned by Fe doping from 3.76 eV to 2.51 eV because of the upward shifting of t_{2g} level. The broad transmittance peak in Fourier transform infra-red spectra at 500 cm^{-1} is assigned to Ni–O stretching vibration mode. Differential scanning calorimetry curve revealed that the transition at 250 °C was exothermic because of structural relaxation. Copyright © VBRI Press.

Keywords: Nickel oxide nanoparticle, XRD, TEM, band gap.

Introduction

Nanoscale oxide particles especially Nickel Oxide nanoparticles are showing attracting properties like mechanical, magnetic, electric and optical properties than its bulk counterpart material and it is also gaining the attention of researchers as these materials are very sensitive and functionally well build [**1**]. The uses of nano catalyst are also gaining importance in the field of nanoscience and nanotechnology in recent days. For organic transformation reactions metal oxide nanoparticles can be used as a heterogeneous catalyst rather a homogenous catalyst. The uses of metal oxide nanoparticles as heterogeneous catalysts are far better over a homogeneous catalyst due to (i) a heterogeneous catalyst is recyclable in novel organic reaction; (ii) a solid heterogeneous catalyst is easily separable from the reaction mixture and (iii) its low cost. However there are some challenges to all the researchers to introduce a clean process and eco-friendly and recyclable nano catalyst for synthesis of organic/inorganic compounds. NiO nanoparticles are now extensively used as a heterogeneous catalyst [**2, 3**]. In this article, efforts are given to improve the properties of the nickel oxide nanomaterials to make those suitable for new applications and devices.

Nanocrystalline nickel oxide (NiO) is also an important transition metal oxide and have a great use in various applications in different fields such as in ceramic, magnetic, catalysis [**4-6**], fuel cell electrodes [**6, 7**], sensors [**8**], electrochromic films [**9-12**], optical fibres, dye sensitized solar cells and optoelectronic nano devices [**13-15**].

Adding dopant into the NiO structure is one of the ways to alter the optical and others physical properties [**16-18**]. The added active elements stabilize the NiO surface and promote a decrease in grain size. Both doped and pure NiO are extensively used because of their low price, easiness of fabrication, good magnetic and optical properties. Most of the researchers are investigating the electrical and magnetic properties of Fe doped NiO NPs [**19**]. Various approaches have been developed to prepare NiO NPs such as sol-gel, anodic arc plasma, electrospining, microemulsion, solvothermal, organic solvent and etc. There are other ways by which we can prepare the NiO nanoparticles which include spray pyrolysis, microwave method, template process and hydrothermal process. Among many other conventional wet chemical processes, auto combustion route is very simple and cost effective for the synthesis of homogeneous, crystalline NiO NPs in a single step shorter reaction times [**20-23**]. In this method NiO NPs are formed and in varying the Fe dopant it affects the size of NiO NPs and its optical properties.

Experiment and characterizations

Synthesis method

Crystalline NPs of $Fe_xNi_{(1-x)}O$ with x = 0.00, 0.03, 0.06, and 0.10 have been synthesized through auto-

combustion route using $Fe(NO_3)_3$, $Ni(NO_3)_2$, and citric acid $[(C_6H_8O_7).H_2O]$ as starting materials. All chemical in this work were of analytical grade reagents without any further purification. In typical synthesis process, citric acid was mixed to 50 ml distilled water to maintain its pH 1.5 at 80 ℃ under magnetic stirring. Then $Fe(NO_3)_3$ and $Ni(NO_3)_2$ in desired amount was dissolved in distilled water and stirring for 2 hour at 80 ℃ in order to form an aqueous uniform solution. When the water was entirely vaporized, the solution transformed into green colour gel then the gel transfer into a combustion bath at 200 ℃. After sometime the gel got fired and grey colour fine powder was formed. Then the powder was ground for 30 minute and annealed at 500 ℃ for 4 hours to improve the crystalline ordering.

Characterizations

The crystal structures and phase for Fe doped NiO NPs were investigated using (Rigaku Miniflex II) Cu-K$_α$ radiations (λ=1.5406 Å) operated at voltage of 30 kV and current 15 mA in 2θ angle range from 20° to 80° with scan rate of 2° /min. The crystallite size has further determined using Debye Scherrer formula from the XRD result. The FTIR spectra of the samples were collected using Perkin Elmer IR Spectrophotometer with KBr pellets in the range of 4000-400cm^{-1} to get the information of different chemical bonding between atoms. The UV-visible spectra were performed in the wavelength range 260-800 nm using Perkin Elmer Spectrophotometer (Lambda 35) to study the optical properties. The surface morphology and shape of the synthesized NPs were recorded by FESEM (FEI Nova Nano). The elemental composition were analysed by EDS equipped with FESEM. To estimate particle size and their formation, we have used Transmission Electron Microscope (JEOL JEM 2100) at operating voltage 200 kV and selected area electron diffraction (SAED) pattern. To study the thermal characteristics and to determine the calcine temperature TGA (Parkin Elmer-Pyris 1) and DSC (Parkin Elmer DSC600) analyses have been performed in a nitrogen atmosphere in the conditions (i) 1 min holding at 50 ℃, (ii) 10 ℃/min temperature raise from 50 to 700 ℃, (iii) 10 min holding at 700 ℃ and (iv) a heating rate of 10 ℃/ min.

Results and discussion

XRD analysis

Fig. 1 displays the XRD patterns of Fe doped NiO NPs calcinated at 500 ℃ and were indexed using PowderX software. These analyses collected information on the full width at half maximum (FWHM) for (1 1 1), (2 0 0), (2 2 0), (3 1 1) crystallographic families to be used to calculate the crystallite size by Debye Scherrer formula [**24**].
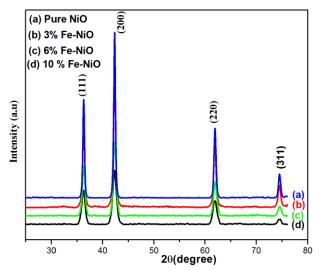

Fig. 1. XRD Pattern of (a) 0%, (b) 3%, (c) 6% and (d) 10 % Fe doped NiO NPs.

All of the peaks match well with Bragg reflections of the standard face centered cubic structure [JCPDS-ICDD: 04-0835, Space group: Fm-3m (225)], the diffraction peaks at 2θ range at 36.26°, 42.27°, 61.94°, and 74.55° can be indexed as (111), (200), (220), and (311) crystal planes, respectively [**24**]. **Fig. 1**(b, c) and (d) shows 3%, 6% and 10% Fe-NiO NPs respectively and their peaks at same position as pure NiO NPs and there is no noticeable peak shift upto 10% Fe doping. The peaks of Fe doped NiO are broaden with increasing the amount of Fe dopant as shown in **Fig. 1**. The intensity of the peaks are going to decrease whereas the width increases indicating the reducing of crystallite size with Fe doping. XRD result revealed that the prepared sample has NiO with cubic FCC structure without any impurity. XRD analysis confirms that single phases of the NiO and Fe-doped NiO NPs have been successfully synthesized using auto combustion method. The average crystallite size was calculated using Scherrer formula:

$$D = \frac{k \times \lambda}{\beta \times \cos\theta} \qquad (1)$$

where, k is shape constant and its value is 0.9 for spherical shape, λ is the wavelength of X-ray radiation, β is full width at half maximum (FWHM) of the highest peak at the diffracting angles θ. The calculated crystallite size of NiO NPs is found to be 21 nm. The crystallite size distribution of Fe-NiO NPs with different doping concentration is shown in **Table 1**. These results show that the Fe doping caused decease in crystallite size of NiO NPs compared to pure NiO NPs, prepared under the same synthesis conditions. This phenomenon can be explained in light of ionic radius. The ionic radii of Ni^{2+} and Fe^{3+} are 0.69 Å and 0.64 Å, respectively. When Fe ions are doped in NiO matrix, they replace the Ni ions from the lattice. Due to the small ionic radii of Fe there is a shrink in the lattice constant which reduces the crystallite size. The difference between the ionic radii provoked a disorder

in the crystalline structure [**25-31**]. We have seen that there is a decrease in the lattice parameter as function of the iron insertion. Due to limited solubility, second phase precipitation is expected at higher concentrations of Fe in NiO [**29**]. Appearance of Fe_2O_3 phase beyond 2% and $NiFe_2O_4$ phase beyond 5% Fe in NiO has been reported [**25**]. But we have successfully synthesized upto 10% Fe doped NiO NPs under the same synthesis condition without any extra impurity or secondary phase peak.

Table 1. Crystallite size of Fe-NiO NPs.

Fe concentration in NiO (mol%)	Crystallite Size (nm)	Lattice parameters a=b=c (Å)
0	21.48	4.1899
3	18.75	4.1895
6	12.71	4.1892
10	10.62	4.1889

SEM and EDS analysis

To study the morphology, the FESEM images of pure and 6 % Fe doped NiO NPs have been shown in **Fig. 2** (a) and (b) respectively. Both figures show the growth of large number of particles aggregate of smaller individual of different sizes. It is confirmed that all the particles are in nano size and the particle size of 6% Fe-NiO NPs is smaller the pure NiO NPs which agreed with XRD results. It is also found that the distribution of pure NiO NPs is less aggregated than that of the doped one which proves that the Fe incorporation creates crystal distortion and reduces the crystalline nature.
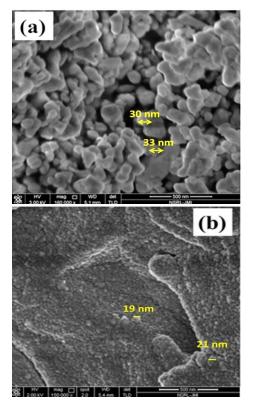

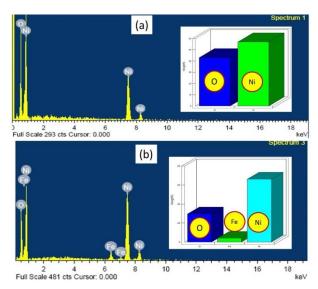**Fig. 2.** FESEM image of (a) pure NiO and (b) 6% Fe doped NiO NPs.

Fig. 3. EDS images of (a) pure and (b) 6 % Fe doped NiO NPs.

Chemical compositions of those both NiO NPs were investigated by energy dispersive X-ray spectroscopy (EDS) and revealed in **Fig. 3(a)** and **(b)**. The EDS analysis stated that both Ni and Fe elements are found in the sample which validates the successful doping of Fe in the NiO host structure and verified the XRD results. Therefore, the synthesis of all Fe doped NiO NPs through auto combustion method was successful.
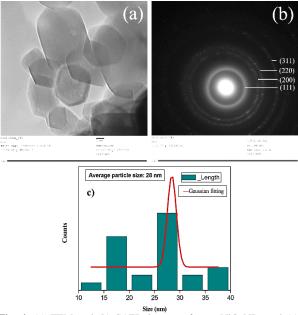

Fig. 4. (a) TEM and (b) SAED images of pure NiO NPs and (c) Average particle size.

TEM analysis

In order to expose the morphology and size of the synthesized Fe doped NiO NPs, the typical TEM images have been recorded, as shown in **Fig. 4(a)**. It can be clearly observed that the synthesized particles are in nano scale range with average size around 28 nm. The particle size obtained from TEM is well matched

with the measured from the XRD results [**32**]. **Fig. 4(b)** shows the selected area electron diffraction (SAED) pattern of Fe doped NiO NPs, which is recorded by focusing the beam on a few particles of the sample. The bright points in SAED pattern confirm the crystalline nature whereas the ring pattern proves the polycrystalline nature of the sample. So the TEM result verifies that Fe is successfully doped in NiO nanostructure without any major lattice defects.
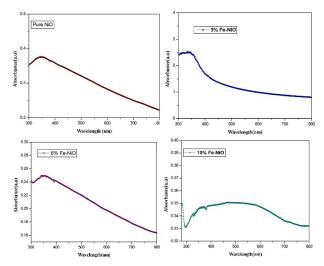

Fig. 5. UV-Visible absorbance spectra for all samples.

Optical analysis

UV–Visible spectroscopy is a very important and useful technique to study the optical properties of semiconducting NPs. Generally, the absorbance depends on several factors such as band gap, oxygen deficiency, particle size and structure of NPs, surface roughness and impurity centres [**33**].

UV-Visible absorption spectra of all Fe doped NiO NPs have been studied with UV-visible Spectrometer (PerkinElmer Lamda35), dispersed in Di-Methyl Sulphoxide (DMSO) by ultrasonicating for 1 hour to make homogeneous dispersion solution. A plot of optical absorbance spectra of all samples are shown in **Fig. 5** as a function of the wavelength. A strong absorption at wave length 330, 360, 390 and 450 nm is observed in NiO NPs for 0%, 3%, 6% and 10% Fe doping, respectively. The absorption edges are found to shift towards higher wavelengths i.e. lower energies with increase in Fe concentration. The optical band gap was evaluated using the Tauc relation [**34**].

$$\alpha h\nu = A(h\nu - E_g)^n \tag{2}$$

$$(\alpha h\nu)^2 = A(h\nu - E_g) \text{ for n=1/2} \tag{3}$$

where, α is the absorption coefficient (α= 2.303 A/t, here A is the absorbance and t is the thickness of the cuvette), hν is the photon energy, and E_g is the optical energy band gap and the value of n = 1/2, 1, 3/2 and 2 is depends on the nature of the transition and n = 1/2 for direct band gap semiconductor. The band gap (E_g) is estimated from the intercept of the linear portion of the curve in the plot of $(\alpha h\nu)^2$ on the Y-axis versus photon

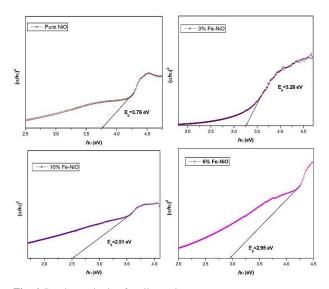energy (hν) on the X-axis as shown in **Fig. 6** and corresponding energy gap are tabulated in **Table 2**.

Fig. 6. Band gap plotting for all samples.

Table 2. Approximate band gap measurement of Fe-NiO NPs.

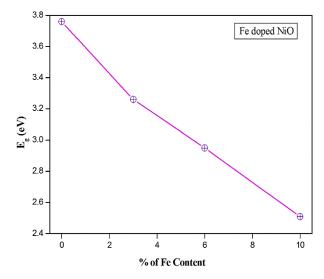| Fe (mol %) in NiO	Band gap Eg(eV)
0	3.76
3	3.26
6	2.95
10	2.51

Fig. 7. Energy band gap (E_g) variation with Fe concentration in NiO NPs.

It has been observed that the energy band gap decreases with a decrease in the lattice parameter. Small changes in the optical band gap with the changes in doping concentration have been shown in **Fig. 7**. The band gap is 3.76 eV for pure NiO NPs which is close to the reported value [**35**] and it decreases for 3, 6 and 10 wt% of Fe doping and found to be 3.26, 2.95 and 2.51 eV respectively. When we doped Fe in NiO then there is an introduction of t_{2g} of Fe level in between top

of valence band and bottom of the conduction as shown in **Fig. 8**. In intrinsic NiO, mixture of Ni e_g and fully occupied t_{2g} comprised the valence band maximum and on the other hand, the Ni e_g comprised the conduction band minimum [**36**]. As Fe has two electrons less than Ni, so when the Fe atoms replaced Ni atoms in NiO, the t_{2g} level of Fe is move up to the Fermi Energy and become the highest fully occupied state. The conduction band minimum remains Ni e_g with no change in the conduction band edge. So, basically due to the upward movement of Fermi energy of t_{2g} level, the band gap continuously decreases, with increasing the doping amount of Fe in NiO [**36**].

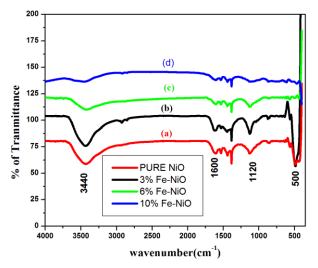**Fig. 8.** Formation of Energy band gap of Fe doped in NiO NPs.

Fig. 9. FTIR spectra of all Fe doped NiO NPs.

FTIR analysis

FTIR is a powerful experimental technique to identify the information about the chemical bonding and also the elemental composition of a material. The recorded FTIR spectra of 0%, 3%, 6% and 10 % Fe doped NiO NPs were as shown in **Fig. 9**. Several significant transmittance peaks are clearly seen in the FTIR spectra. The broad absorption band at 500 cm^{-1} is assigned to Ni–O stretching vibration mode [**40, 41**].

Besides the Ni–O vibration, in **Fig. 9**, one broad absorption band around at 3440 cm^{-1} can be observed. The band can be assigned to the O–H stretching vibrations and the other weak band near 1600 cm^{-1} can be attributable to H–O–H bending vibrations mode, due to the adsorption of water from air during the preparation of sample pellet in the open air [**42**]. The peaks in the region of 1000– 1500 cm^{-1} can be attributed to the C–O stretching vibration and O–C=O symmetric and asymmetric stretching vibrations [**43**]. The weakening intensity of the band indicates that the ultrafine powers tend to strong physically absorption to CO_2 and H_2O [**44**].

TGA and DSC analysis

Thermogravimetric analysis (TGA) was carried out using a ParkinElmer (Pyris 1) Thermal Analyser. DSC analysis was carried out using ParkinElmer DSC600.

The TGA analysis is used to study the thermal characteristics of the product. The typical TGA curve of NiO nanomaterials is shown in **Fig. 10 (a)**. It can be observed that the weight loss happens in two temperature regions: (1) 50-250 °C and (2) 250-450 °C. But clearly we see from TGA curve that only 9 % weight loss of the total weight of NiO has been occurred. The first weight loss between 50 and 250 °C temperature region can be assigned to the evaporation of the absorbed water. The second weight loss occurs between 250 °C and 450 °C region, which can be attributed to the conversion of $Ni(OH)_2$ into NiO which was present in NiO sample. Above 400 °C, the TG curve become flat [**45**]; obviously there is no change in the weight of the NiO on the TGA curve. It leads to choose the calcine temperature [**32**].
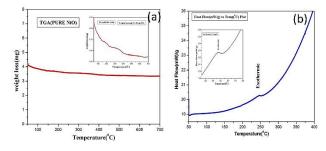
Fig. 10. (a) and (b) (TG/DSC) graphs of (nickel hydroxide) nickel oxide NPs.

The region at 250 °C exhibits only a slight weight loss, which may be due to the further removal of chemisorbed water through the conversion of $Ni(OH)_2$ to NiO; however, this weight loss is accompanied by a exothermic heat flow which is shown in **Fig. 10(b)**. This heat flow is believed to be due to structural relaxation [**46**], where pores are eliminated without significant weight loss. During the structural relaxation of the NiO, the surface area and pore volume decrease sharply and particles become more crystalline [**47**].

At 250 °C, TGA exhibits a slight weight loss about 9% of the initial mass due to the removal of hydroxyl groups bound loosely in surface, with a sharp increase in the weight loss at and beyond 250 °C. The reactions accompanying the transition at 250 °C was highly exothermic because of structural relaxation.

Conclusion

In summary, Fe doped NiO NPs with an average crystallite size of 28 nm have been successfully synthesized through gel combustion technique and an investigation on their optical and structural properties was also carried out. The XRD, EDS and TEM results suggested the formation of single-phase polycrystalline Fe-NiO NPs without any impurities. The optical band gap of NiO NPs is varying from 3.76 eV to 2.51 eV with Fe doping. Thus, this work suggested that the optical properties and band gap of NiO NPs can be tuned by Fe doping which leads to its applications in various Light Emitting Diode, several nano-optoelectronics devices, displays and smart windows. Also, there have potential applications for heterogeneous catalyst, poultry protection, in UV detection and warming coatings, antireflection coatings and solar control.

References

1. Moura K.O.; Lima R.J.S.; Jesus C.B.R.; Duque J.G.S.; Meneses C.T.; *Rev. Mex. Fis.*, **2012**, *58*, 167.
2. Tanna J.A.; Chaudhary R.G.; Gandhare N.V.; Rai A.R.; Juneja H.D.; *International Journal of Scientific & Engineering Research*, **2015**, *6*, 93.
3. Chaudhary R.G.; Tanna J.A.; Mondal A.; Gandhare N.V.; Juneja H.D.; *Journal of the Chinese Advanced Materials Society*, **2017**, *5*, 103.
4. Berchmans S.; Gomathi H.; Rao G.P.; *J. Electroanal. Chem.*, **1995**, *394*, 267.
5. Gardes G.E.E.; Pajonk G.M.; Teichner S.J.; *J. Catal.*, **1974**, *33*, 145.
6. Dooley K.M.; Chen S.Y.; Ross J.R.H.; *J. Catal.*, **1994**, *145*, 402.
7. Tomczyk P.; Mordarski G.; Oblakowski J.; *J. Electroanal. Chem.*, **1993**, *353*, 177.
8. Makkus C.R.; Hemmes K.; Wir D.W.; *J. Electrochem. Soc.*, **1994**, *141*, 3429.
9. Salimi A.; Noorbakhsh A.; Semnani A.; *J Solid State Electrochem.*, **2011**, *15*, 2041.
10. Chigane M.; Ishikawa M.; *J. Chem. Soc. Faraday Trans.*, **1992**, *88*, 2203.
11. Jiao Z.; Wu M.; Qin Z.; Xu H.; *Nanotechnology*, **2003**, *14*, 458.
12. Kitao M.; Izawa K.; Urabe K.; Komatsu T.; Kuwano S.; Yamada S.; *Jpn. J. Appl. Phys.*, **1994**, *33*, 6656.
13. Kim S.S.; Park K.W.; Yum J.H.; Sung Y.E.; *Sol. Energy Mater. Sol. Cells*, **2006**, *90*, 254.
14. Borgstrom M.; Blart E.; Boschloo G.; Mukhtar E.; Hagfeldt A.; Hammarstrom L.; Odobel F.; *J. Phys. Chem. B*, **2005**, *109*, 22928.
15. Juarez A.S.; Silver A.T.; Ortiz A.; *Sol. Energy Mater. Sol. Cells*, **1998**, *52*, 301.
16. Ponnusamy P.M.; Agilan S.; Muthukumarasamy N.; Senthil T.S.; Rajesh G.; Venkatraman M.R.; Velauthapillai D.; *Materials Characterization*, **2016**, *114*, 166.
17. Hassan M.M.; Khan W.; Azam A.; Naqvi A.H.; *J. Lumin.*, **2014**, *145*, 160.
18. Panda N.R.; Acharya B.S.; Singh T.B.; Gartia R.K.; *J. Lumin.*, **2013**, *136*, 369.
19. Wolf S.A.; Awschalom D.D.; Buhrman R.A.; Daughton J.M.; Molnar S.V.; Roukes M.L.; Chtchelkanova A.Y.; Treger D. M.; *Science*, **2001**, *294*, 1488.
20. Mondelaers D.; Vanhoyland G.; Van Den Rul H.; D'Haen J.; Van Bael M.K.; Mullens J.; Van Poucke L.C.; *Materials Research Bulletin*, **2002**, *37*, 901.
21. Mentus S.; Tomic-Tucakovic B.; Majstorovic D.; Dimitrijevic R.; *Mater. Chem. Phys.*, **2008**, *112*, 254.
22. Li Y.; Li G.; Yin Q.; *Mater. Sci. Eng. B*, **2006**, *130*, 264.
23. Cheng-Hsiung P.; Chyi-Ching H.; Ching K.H.; San-Yuan C.H., *Mater. Sci. Eng. B*, **2004**, *107*, 295.
24. Mallick P.; Rath C.; Biswal R.; Mishra N.C.; *Indian J. Phys.*, **2009**, *83*, 517.
25. Wang J.; Cai J.; Lin Y.H.; Nan C.W.; *Appl. Phys. Lett.*, **2005**, *87*, 202501.
26. Kodama R.H.; Makhlouf S.A.; Berkowitz A.E.; *Phys. Rev. Lett.*, **1997**, *79*, 1393.
27. Nowotny J.; Rekas M.; *Solid State Ionics*, **1984**, *12*, 253.
28. Battle P.D.; Cheetham A.K.; Gehring G.A.; *J. Appl. Phys.*, **1979**, *50*, 7578.
29. Kurzawa M.; Blonska-Tabero A.; *J. Therm. Anal. Calorim.*, **2004**, *77*, 65.
30. Schweika W.; Hoser A.; Martin M.; Carlsson A.E.; *Phys. Rev. B*, **1995**, *51*, 15771.
31. Anderson A.B.; Grimes R.W.; Heuer A.H.; *J. Solid State Chem.*, **1984**, *55*, 353.
32. Alagiri M.; Ponnusamy S.; Muthamizhchelvan C.; *J. Mater. Sci: Mater. Electron*, **2012**, *23*, 728.
33. Ahmed A.S.; Shafeeq M.M.; Singla M.L.; Tabassum S.; Naqvi A.H.; Azam A.; *J. Lumin.*, **2010**, *131*, 1.
34. Tauc J.; Amorphous and Liquid Semiconductors, *Plenum Press, New York*, **1974**, 171.
35. Boschloo G.; Hagfeldt A.; *J. Phys. Chem. B.*, **2001**, *105*, 3039.
36. Petersen J.E.; Twagirayezu F.; Scolfaro L.M.; Borges P.D.; Geerts W.J.; *AIP Advances*, **2017**, *7*, 055711.
37. Song X.; Gao L.; *J. Am. Ceram. Soc.*, **2008**, *91*, 3465.
38. Tan T.L.; Lai C.W.; Hamid S.B.A.; *J. Nanomater.*, **2014**, *2014*, 1.
39. Viswanatha R.; Sapra S.; Gupta S.S.; et al., *J. Phys. Chem. B*, **2004**, *108*, 6303.
40. Guan H.; Shao C.; Wen S.; Chen B.; Gong J.; Yang X.; *Inorg. Chem. Commun.*, **2003**, *6*, 1302.
41. Patil P.S.; Kadam L.D.; *Appl. Surf. Sci.*, **2002**, *199*, 211.
42. Hassan M.M.; Ahmed A.S.; Chaman M.; Khan W.; Naqvi A.H.; Azam A.; *Mater. Res. Bull.*, **2012**, *47*, 3952.
43. Hassan M.M.; Khan W.; Azam A.; Naqvi A.H.; *J. Indus. Eng. Chem.*, **2015**, *21*, 283.
44. Alaria J.; Turek P.; Bernard M.; Bouloudenine M.; Berbadj A.; Brihi N.; *Chem. Phys. Lett.*, **2005**, *415*, 337.
45. Ghosh M.; Biswas K.; Sundaresana A.; Rao C.N.R.; *J. Mater. Chem.*, **2006**, *16*, 106.
46. Scherer G.W.; Relaxation in Glasses and Composites, *Wiley New York*, **1986**.
47. Lin C.; Al-Muhtaseb S.A.; Ritter J.A.; *J. Sol-Gel Sci. Technol.*, **2003**, *28*, 133.